Nonlinear Optics (WiSe 2018/19)
Lecture 11: January 11, 2018

11 Terahertz generation and applications
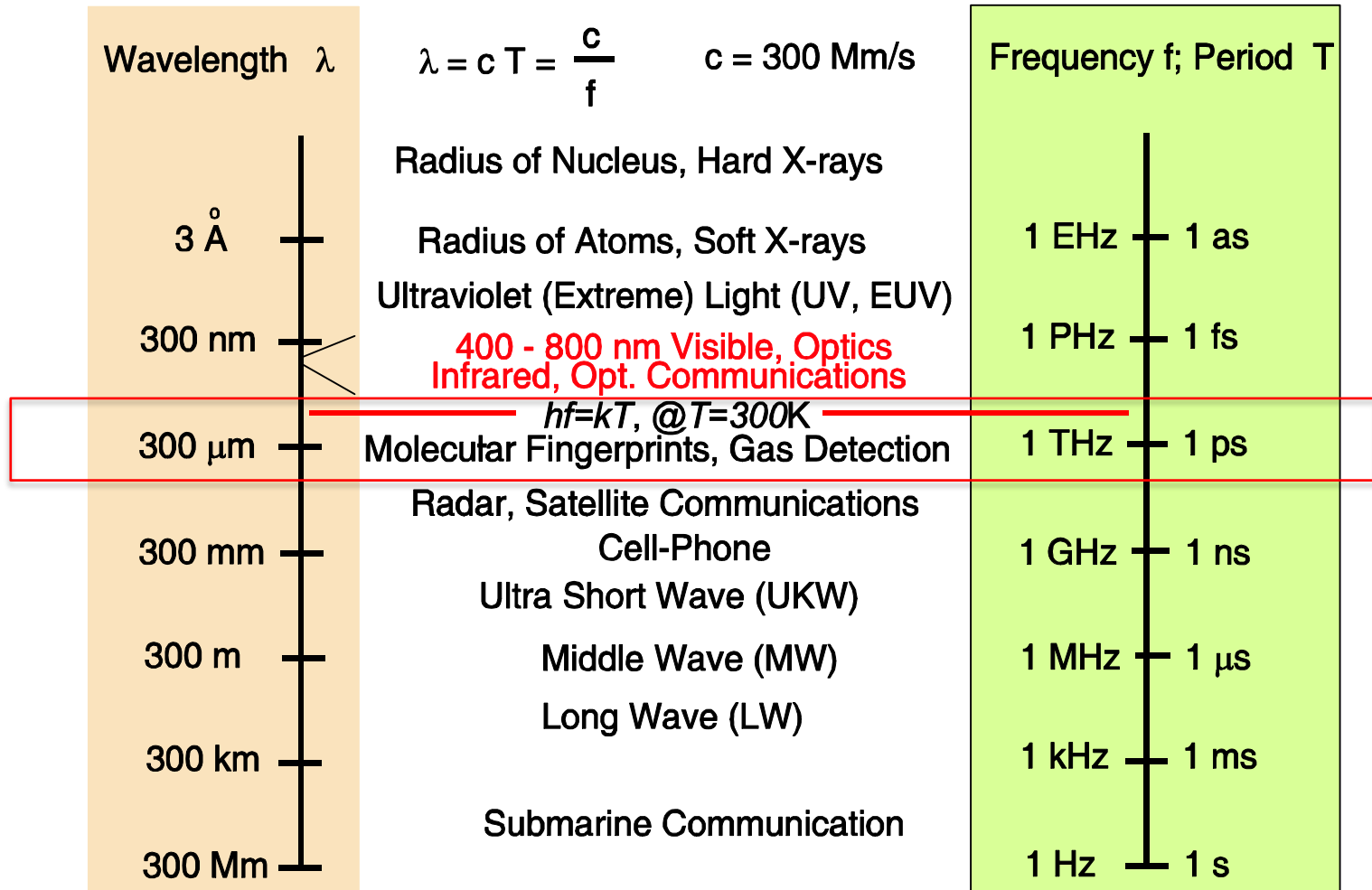
11.1 Auston switch

11.2 Optical rectification

11.2.1 Optical rectification with tilted-pulse-fronts

11.2.2 Optical rectification by Quasi-Phase Matching (QPM)

11 Terahertz generation and applications

Wavelength λ	$\lambda = c\,T = \dfrac{c}{f}$ c = 300 Mm/s	Frequency f; Period T
	Radius of Nucleus, Hard X-rays	
3 Å	Radius of Atoms, Soft X-rays	1 EHz — 1 as
	Ultraviolet (Extreme) Light (UV, EUV)	
300 nm	400 - 800 nm Visible, Optics	1 PHz — 1 fs
	Infrared, Opt. Communications	
	$hf=kT$, @T=300K	
300 μm	Molecular Fingerprints, Gas Detection	1 THz — 1 ps
	Radar, Satellite Communications	
300 mm	Cell-Phone	1 GHz — 1 ns
	Ultra Short Wave (UKW)	
300 m	Middle Wave (MW)	1 MHz — 1 μs
	Long Wave (LW)	
300 km		1 kHz — 1 ms
	Submarine Communication	
300 Mm		1 Hz — 1 s

0.3 – 30 THz

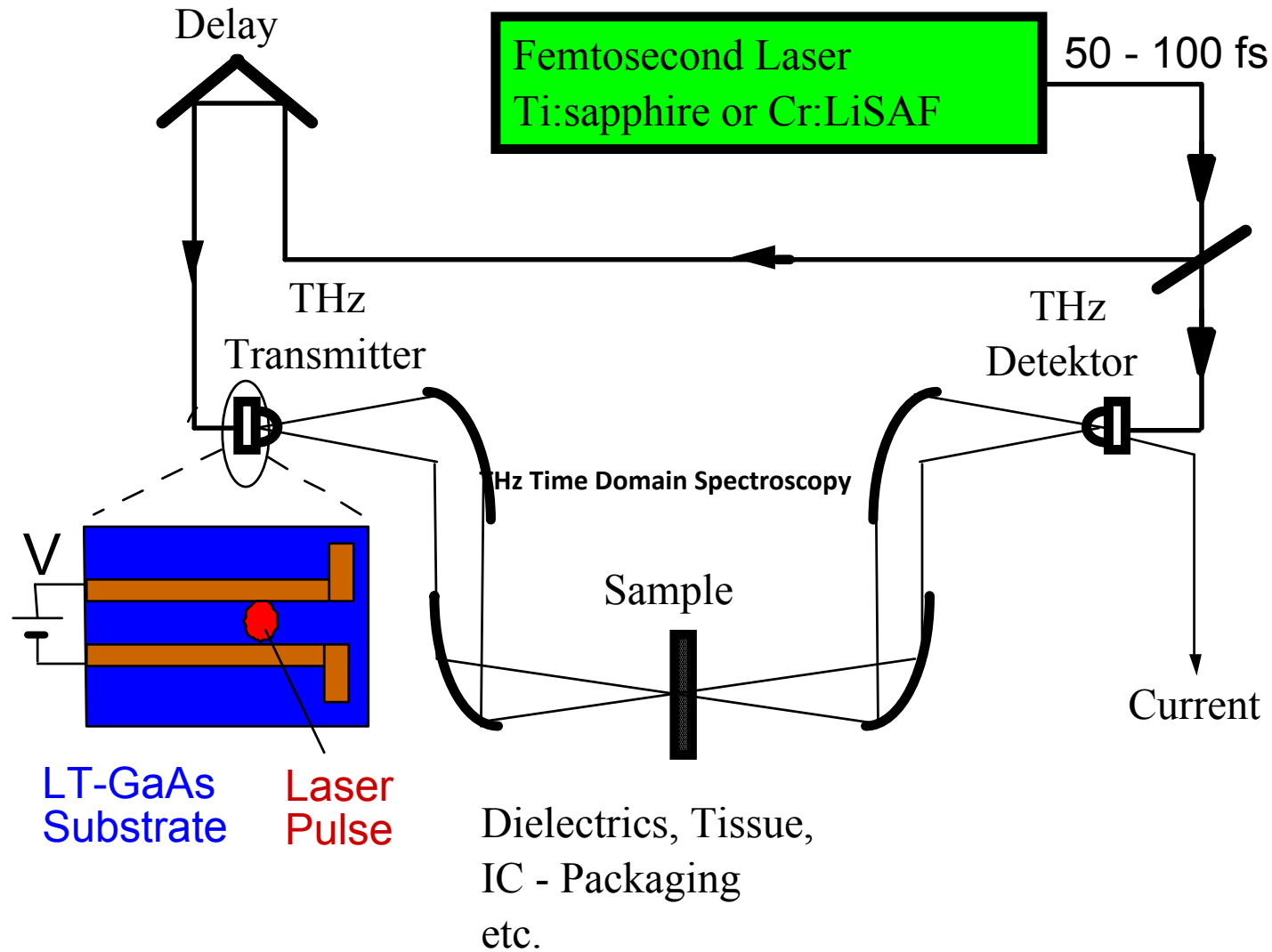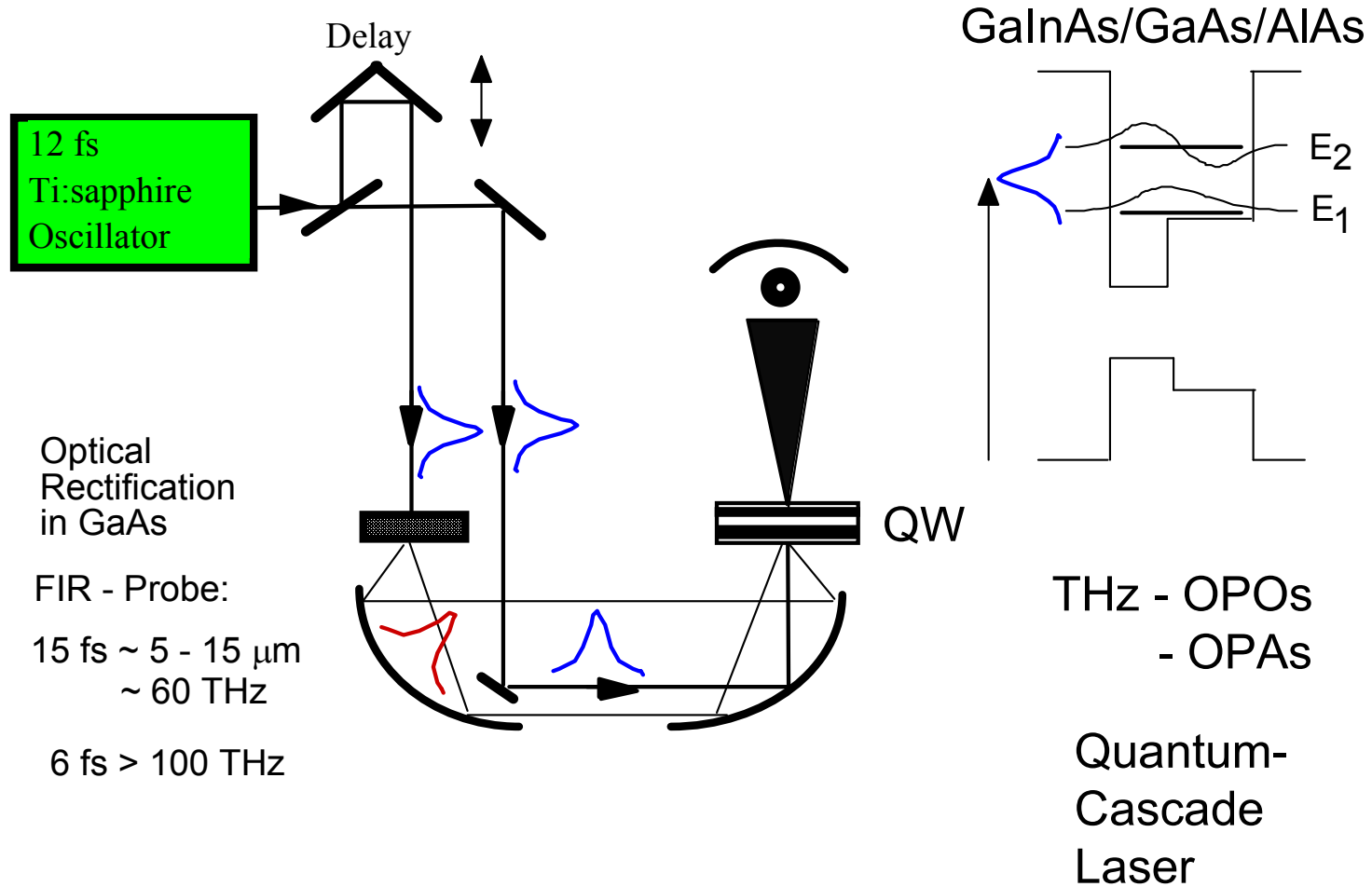# THz Time Domain Spectroscopy

Fig. 11.1: THz pulses generated (a) and received (b) with photoconductive switches.

THz Time Domain Spectroscopy using optical rectification in GaAs

Delay

12 fs
Ti:sapphire
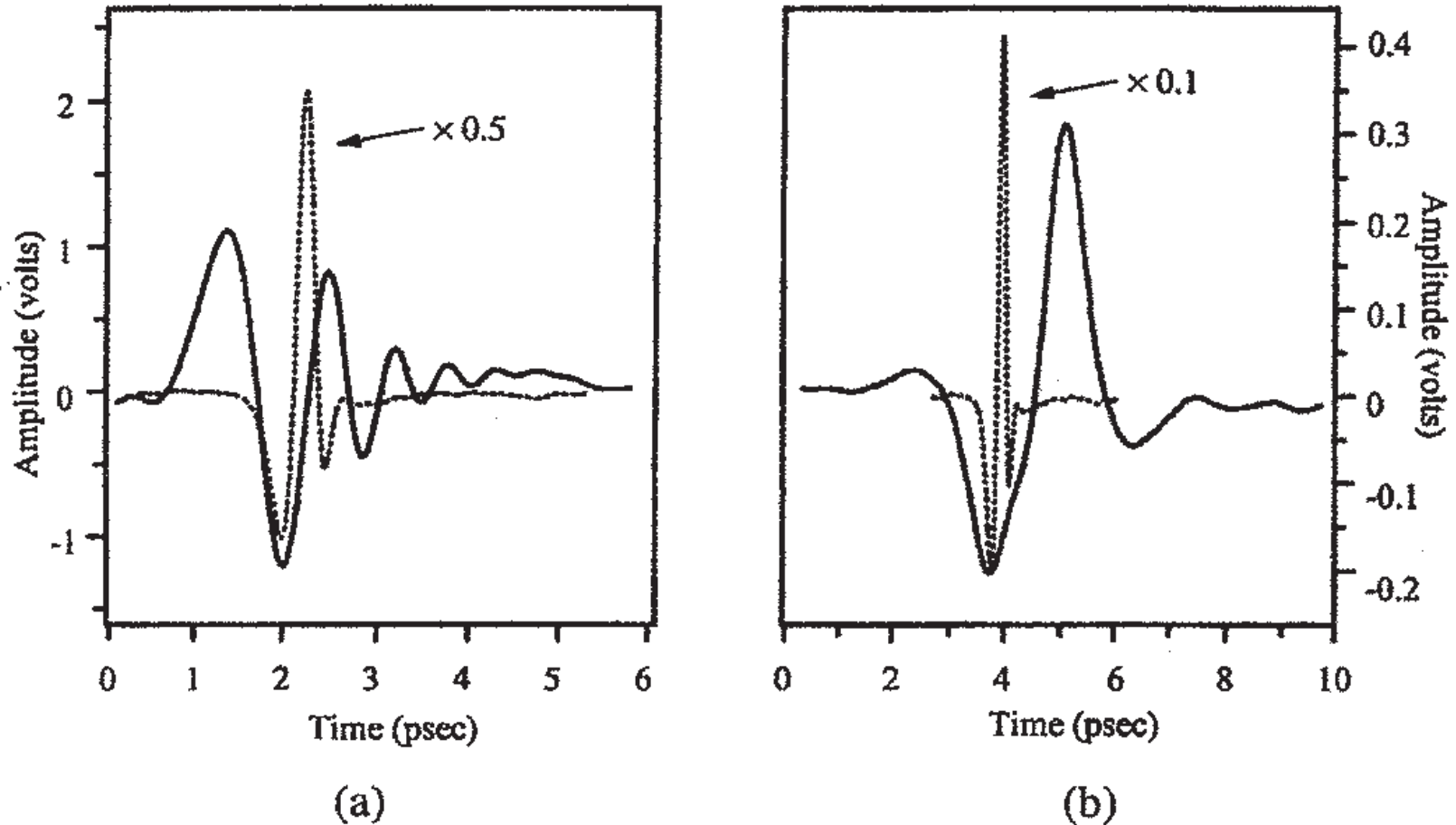Oscillator

Optical
Rectification
in GaAs

FIR - Probe:

15 fs ~ 5 - 15 μm
~ 60 THz

6 fs > 100 THz

QW

GaInAs/GaAs/AlAs

E_2

E_1

THz - OPOs
- OPAs

Quantum-
Cascade
Laser

Time Domain THz Spectroscopy

Figure 11.2: Terahertz waveforms modified by passage through (a) a 10 mm block of stycast and (b) a chinese fortune cookie. The dashed lines show the shape of the input waveform multiplied by 0.5 in (a) and by 0.1 in (b). In (a) the transmitted pulse exhibits a strong "chirp" due to a frequency-dependent index, while in (b), pulse broadening indicates preferential absorption of high frequencies. [7]

Attosecond diffraction and spectroscopy of biomolecules
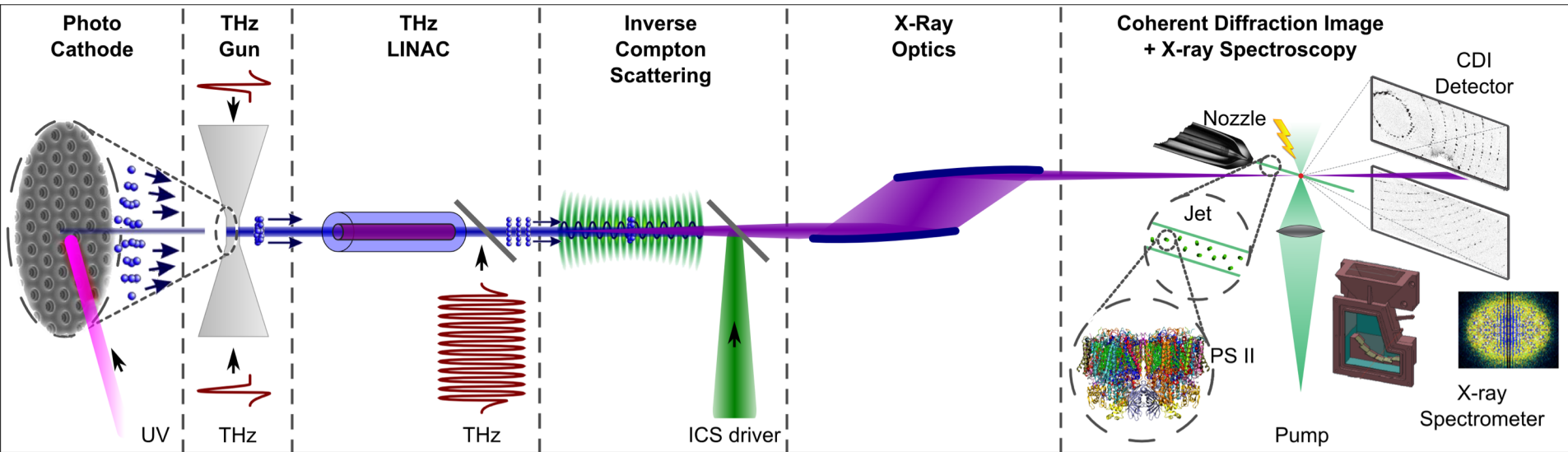
All laser driven, intrinsic attosecond synchronization

Only pico-second lasers at 1J-level necessary -> kHz operation

→ All optical driven fully coherent attosecond X-ray source:
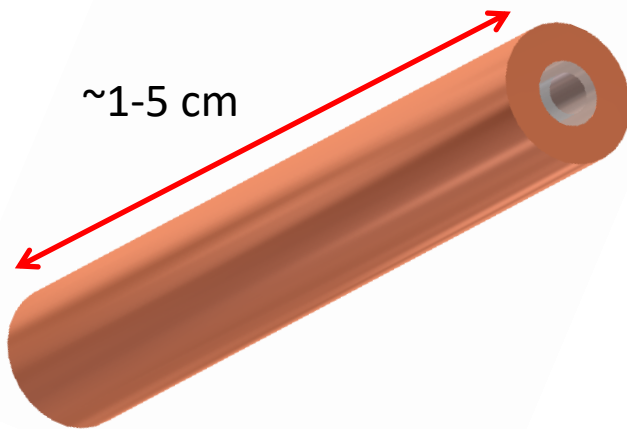
→ has its own science case

→ seeding of large scale FELs

→ resolve access problem to large facilities
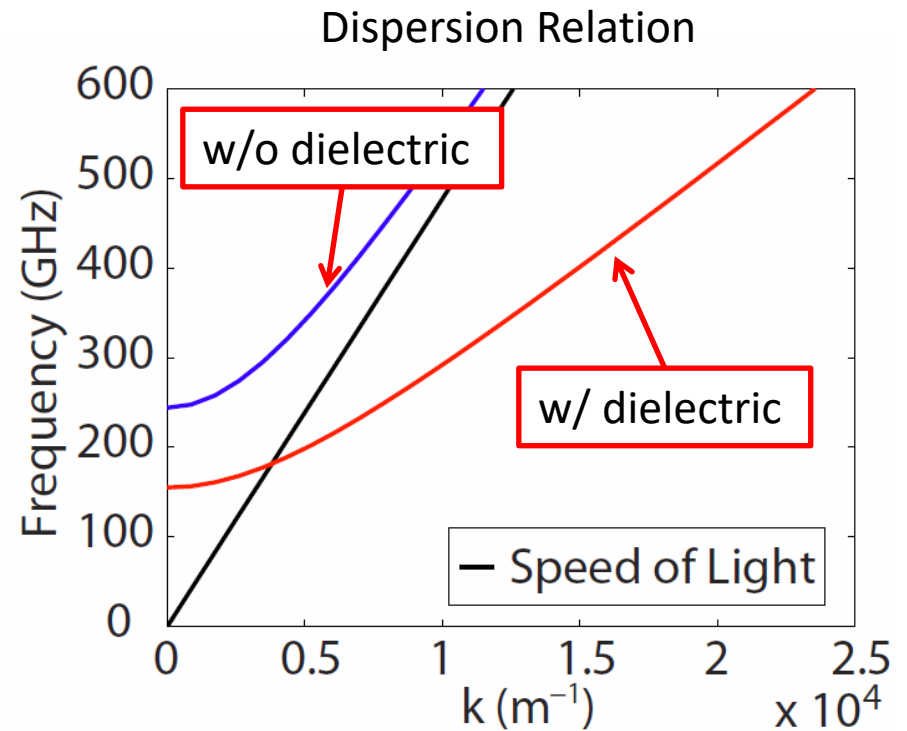
THz Acceleration

Dielectrically Loaded Circular Waveguide

- Traveling wave structure is best for coupling broad-band single cycle pulses
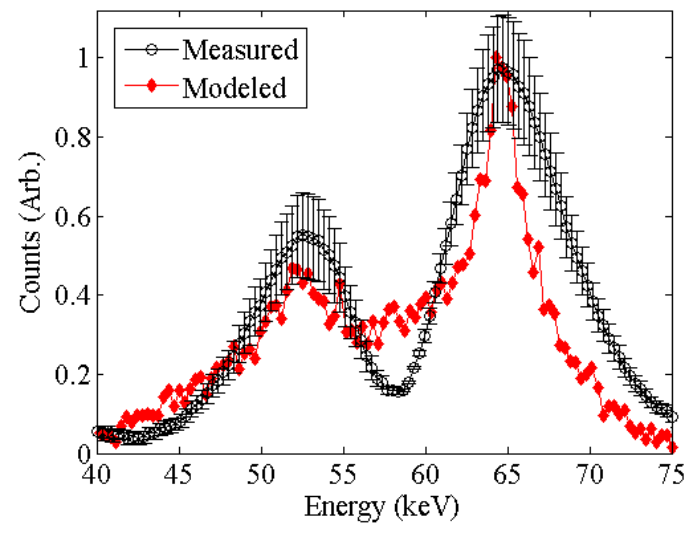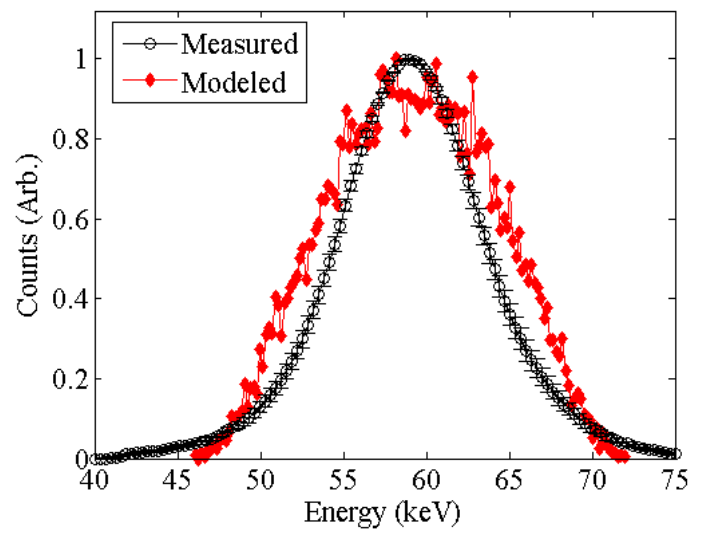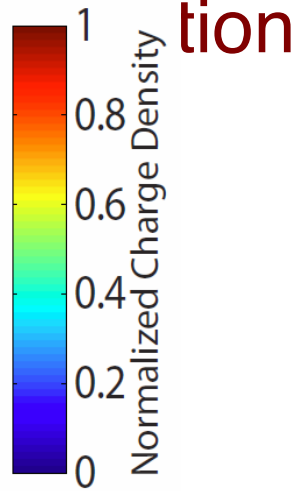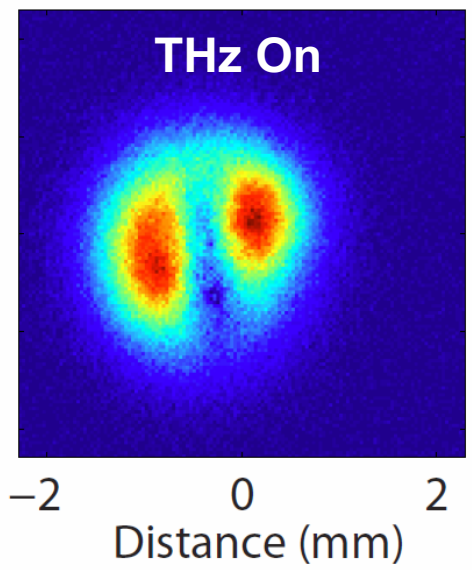- Phase-velocity matched to electron velocity with thickness of dielectric

~1-5 cm

Copper Inner Diameter = 940 μm

Fused Silica Inner Diameter = 400 μm

Dispersion Relation

w/o dielectric

w/ dielectric

— Speed of Light

Frequency (GHz)

k (m^{-1})   x 10^4

L.J. Wong et al., Opt. Exp. 21, 9792 (2013).   **7**
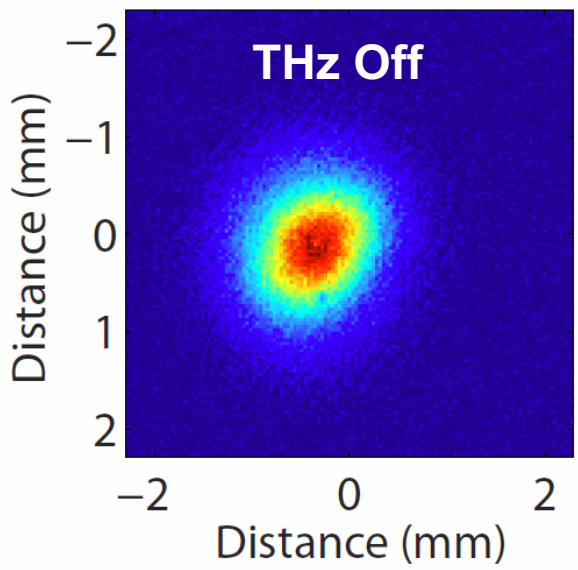
11.2 Optical rectification

Figure 11.3: THz generation by DFG from two cw lines or from intrapulse spectral components. Once intense enough THz has been generated it acts back on the generating lines and creates addit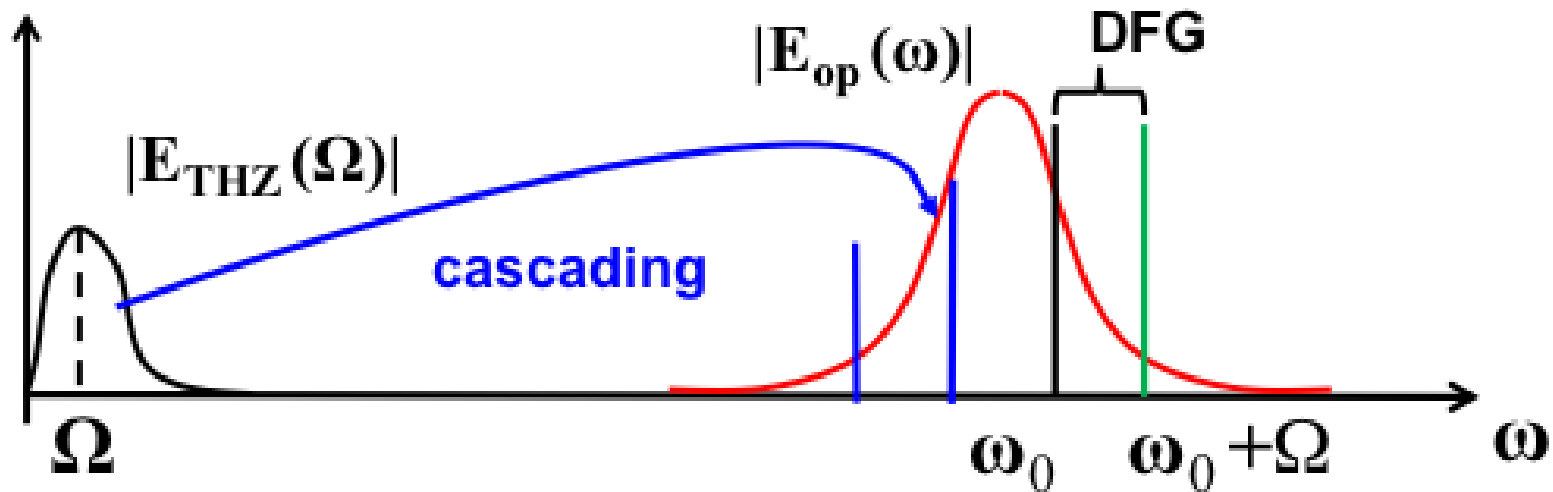ional down-shifted lines, which themselves again generate THz by DFG. This cascaded DFG process leads to a continuous down- shifting of the center of the optical spectrum.

THz Materialproperties I

crystal	ZnTe	LiNbO$_3$	LiTaO$_3$	GaP
opt. wl (μm)	0.8	1.06	1.06	1.06
opt. ref. index	2.85	2.16	2.14	3.11
THz ref. index	3.2	5.2	6.5	3.21
$\Delta n = n_{THz} - n_{g,opt}$	0.35	3.0	4.32	0.1
THz abs. (cm^{-1})	9.9	21.7	95	3.3
transp. range (μm)	0.55-30	0.4-5.2	0.4-5.5	0.55-10
band gap (eV)	2.26	3.7	5.65	2.25
nonlin. coeff. (pm/V)	d$_{14}$=23.1	d$_{33}$=152.4	d$_{33}$=145.2	d$_{14}$=21.7
nonlin. ref. index n$_2$ $\frac{10^{-15}\text{cm}^2/\text{W}}{\text{at } \lambda \ (\mu\text{m})}$	120 at 1.06 71 at 0.8	0.91 at 1.06	0.37 at 1.06	20 at 0.78
FOM$_1$, long pulses	0.03	1	0.21	0.06
FOM$_2$, ultrashort pl.	0.74	1	0.64	1,67
FOM$_3$, Kerr-limited	0.00045	1	0.416	0.005

Table 11.1: Linear and nonlinear properties, and figures of merit (normalized to LiNbO$_3$) of crystals transparent in the 0-4 THz range and most widely used for optical THz generation according to Ref. [10].

THz Materialproperties II

crystal	GaSe	GaAs	ZGP	CdSiP$_2$
opt. wl (μm)	1.06	2.1	2.1	2.0
opt. ref. index	2.8	3.33	3.15	3.0
THz ref. index	3.26	3.6	3.37	3.05
$\Delta n = n_{THz} - n_{g,opt}$	0.34	0.18	0.17	0.05
THz abs. (cm^{-1})	2.5	1	1	<0.1
transp. range (μm)	0.65-18	0.9-15	0.75-12	0.5-9
band gap (eV)	2.1	1.424	2.34	2.45
nonlin. coeff. (pm/V)	d$_{22}$=24.3	d$_{14}$=46.1	d$_{36}$=39.4	d$_{36}$=85
nonlin. ref. index n$_2$ $\frac{10^{-15}\mathrm{cm}^2/\mathrm{W}}{\text{at } \lambda \ (\mu m)}$	45 at 1.06	150 at 2.1	40 at 2.1	? at 2.1
FOM$_1$, long pulses	0.13	0.83	0.68	
FOM$_2$, ultrashort pl.	0.13	0.64	0.55	
FOM$_3$, Kerr-limited	0.004	0.014	0.047	

Table 11.2: Linear and nonlinear properties, and figures of merit (normalized to LiNbO3) of crystals transparent in the 0-4 THz range and most widely used for optical THz generation according to ref. [10]

Three Wave Interaction

$$\frac{d\hat{E}(\omega_1)}{dz} = -j\kappa_1 \hat{E}(\omega_3)\hat{E}^*(\omega_2)e^{-j\Delta kz},$$

$$\frac{d\hat{E}(\omega_2)}{dz} = -j\kappa_2 \hat{E}(\omega_3)\hat{E}^*(\omega_1)e^{-j\Delta kz},$$

$$\frac{d\hat{E}(\omega_3)}{dz} = -j\kappa_3 \hat{E}(\omega_1)\hat{E}(\omega_2)e^{+j\Delta kz},$$

$$\kappa_i = \omega_i d_{eff}/n_i c_0, \qquad \text{and} \qquad \Delta k = k_3 - k_1 - k_2.$$

Difference Frequency Generation

$$\omega_3 = \omega_0 + \Omega \text{ and } \omega_2 = \omega_0,$$

$$\Omega \text{ is a THz frequency}$$

Phase Mismatch (for collinear interaction)

$$\Delta k = \left. \frac{\partial k_{opt}(\omega)}{\partial \omega} \right|_{\omega_0} \Omega - k_{THz}(\Omega) = \left(\frac{1}{v_{g,opt}} - \frac{1}{v_{p,THz}} \right) \Omega$$

$$= \frac{\Omega}{c} \left(n_{g,opt} - n_{p,THz} \right).$$

For Lithium Niobate   **2**   **5**

→ **Broadband non collinear phase matching by tilted pulse fronts**

→ **Quasi-phase matching**

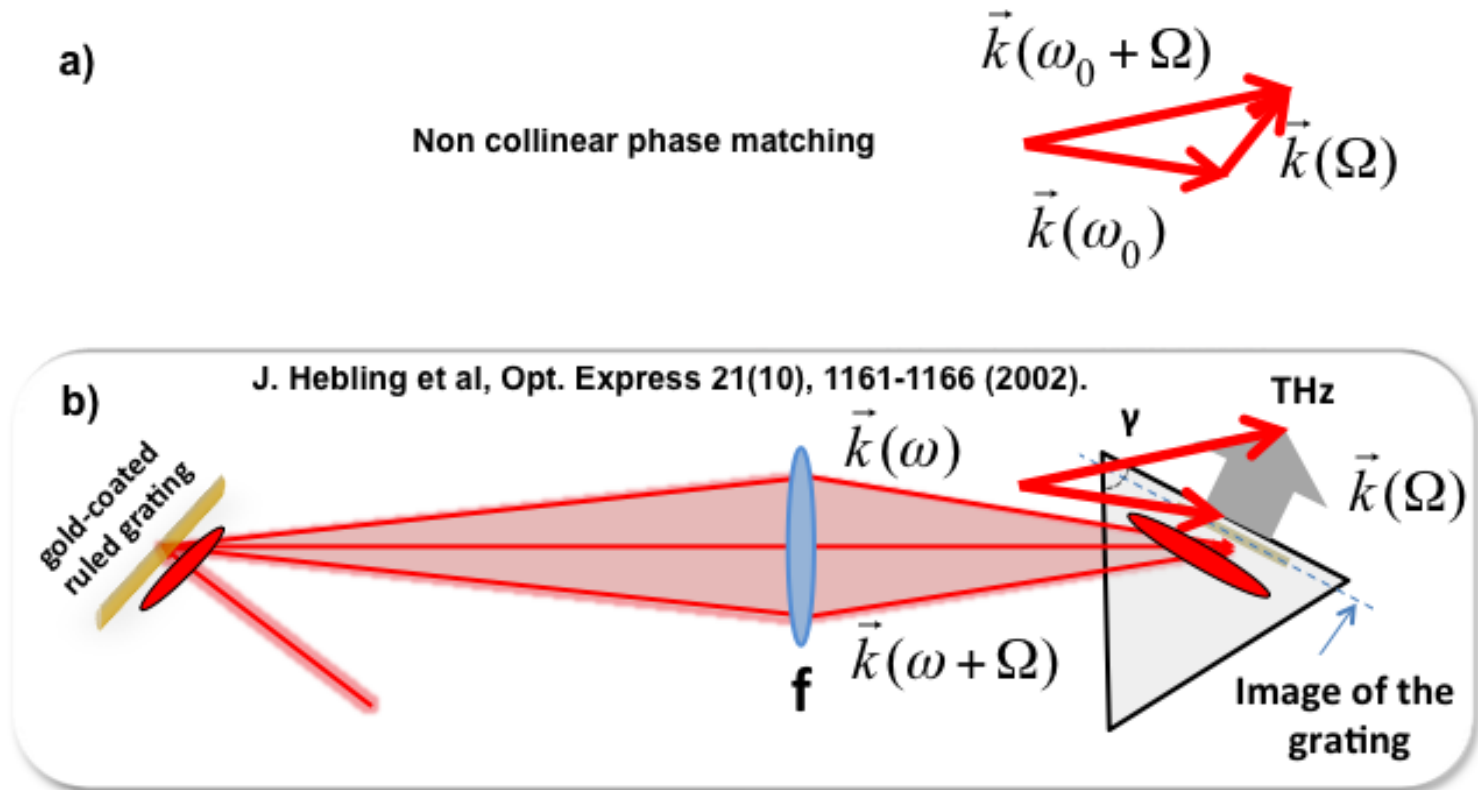# 11.2.1 Optical rectification with tilted-pulse-fronts

a)

Non collinear phase matching

$$\vec{k}(\omega_0 + \Omega)$$

$$\vec{k}(\Omega)$$

$$\vec{k}(\omega_0)$$

b)

J. Hebling et al, Opt. Express 21(10), 1161-1166 (2002).

gold-coated ruled grating

$$\vec{k}(\omega)$$

THz

γ

$$\vec{k}(\Omega)$$

**f** $\vec{k}(\omega + \Omega)$

Image of the grating

Figure 11.4: (a) Noncollinear phase matching for THz generation. Note, the THz phase index in lithium niobate is more than twice as large as the optical group index. (b) Broadband implementation of the noncollinear phase matching using a grating and imaging system that leads to the generation of pulses with a tilted pulse front.

Tilted pulse front technique

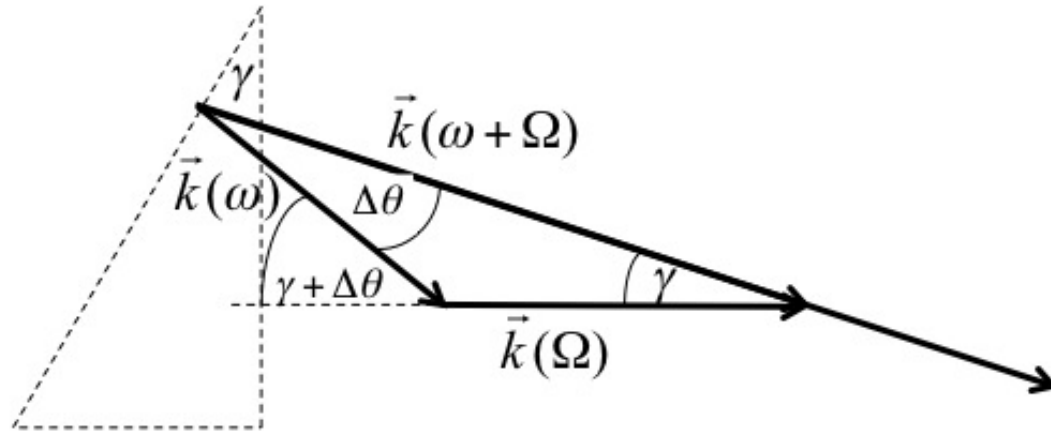
(a)

(b)
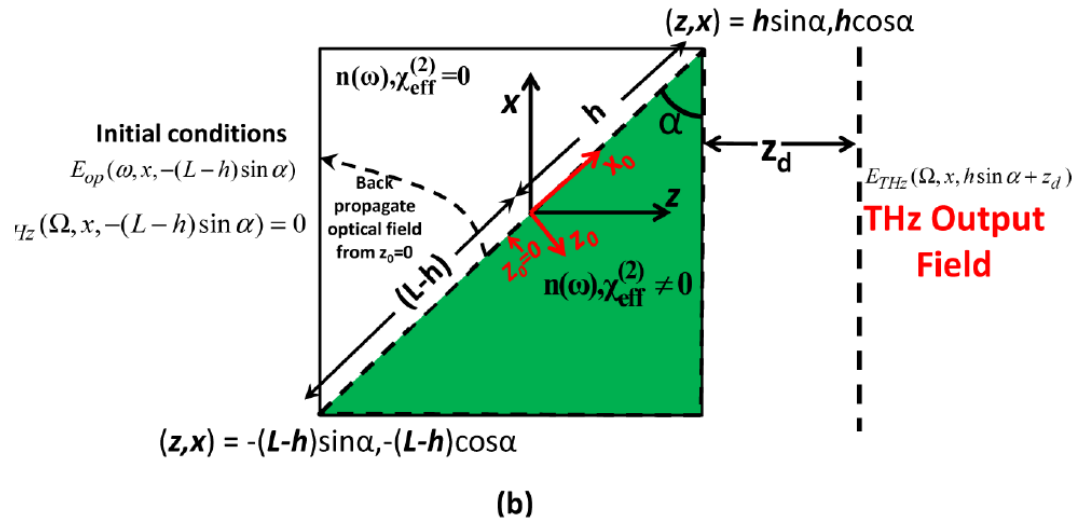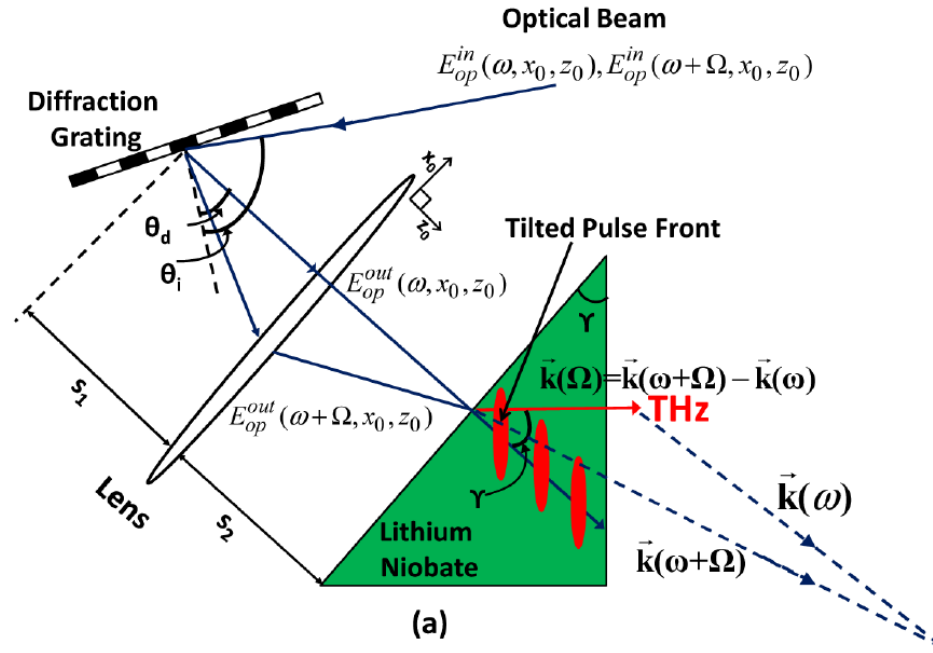
Non-collinear phase matching

Figure 11.6: Noncollinear phase-matching condition for pulse-front-tilted optical rectification.

z - component

$$
\begin{aligned}
\Delta k_z(\omega) &= \cos\gamma \; k(\omega+\Omega) - \cos(\gamma+\theta(\omega)) \; k(\omega) - k_{THz}(\Omega) \\
&= \cos\gamma \; \frac{\partial k_{opt}(\omega)}{\partial\omega}\Omega + \sin\gamma \left(-\frac{\partial\theta}{\partial\omega}\right)\Omega \; k(\omega) - k_{THz}(\Omega) = 0,
\end{aligned}
$$

y - component

$$
\begin{aligned}
\Delta k_y(\omega) &= \sin\gamma \; k(\omega+\Omega) - \sin(\gamma+\theta(\omega)) \; k(\omega) \\
&= \sin\gamma\frac{\partial k_{opt}(\omega)}{\partial\omega}\Omega - \cos\gamma\frac{\partial\theta}{\partial\omega}\Omega \; k(\omega) \\
&= \sin\gamma\frac{\partial k_{opt}(\omega)}{\partial\omega}\Omega - \cos\gamma\left(-\frac{\partial\theta}{\partial\omega}\right)\Omega \; k(\omega) = 0.
\end{aligned}
$$

Tilt angle

$$\frac{\partial k_{opt}(\omega)}{\partial \omega}\Omega - \cos\gamma\, k_{THz}\left(\Omega\right) = 0$$

$$\frac{1}{v_{g,opt}} - \frac{1}{v_{p,THz}}\cos\gamma = 0$$

$$n_{g,opt} = n_{p,THz}\,\cos\gamma,$$

Necessary angular spread

$$\frac{\partial\theta}{\partial\omega} = -\tan\gamma\frac{v_{p,opt}}{\omega\,\,v_{g,opt}} = -\tan\gamma\frac{n_{g,opt}}{\omega\,\,n_{p,opt}}.$$

1D – spatial Model

$$k(\omega) = \frac{1}{\cos\gamma}\frac{\omega\,\,n(\omega)}{c} + \frac{(\omega-\omega_0)^2}{2}k_{AD}^{''}$$

$$k_{AD}^{''} = \frac{-n_{g,opt}^2(\omega_0)}{\omega_0\,\,c\,(\omega_0)}\tan^2\gamma.$$

1D - Model

$$\frac{d\hat{E}_{THz}(\Omega, z)}{dz} = -\frac{\alpha_{THz}(\Omega)}{2}\hat{E}_{THz}(\Omega, z) \tag{11.13}$$

$$-j\frac{\Omega\ d_{eff}}{c\ n_{p,THz}}\int_0^\infty \hat{E}_{opt}(\omega + \Omega, z)\ \hat{E}_{opt}(\omega, z)^* e^{j\Delta k(\omega)z}d\omega\ .$$

which also includes the THz absorption. For the optical field, we obtain

$$\frac{d\hat{E}_{opt}(\omega, z)}{dz} = -\frac{\alpha_{opt}(\Omega)}{2}\hat{E}_{opt}(\omega, z)$$

$$-j\frac{\omega\ d_{eff}}{c\ n_{p,opt}}\int_0^\infty \hat{E}_{opt}(\omega + \Omega, z)\ \hat{E}_{THz}(\Omega, z)^*\ d\Omega e^{-j\Delta k(\omega)z}$$

$$-j\frac{\omega\ d_{eff}}{c\ n_{p,opt}}\int_0^\infty \hat{E}_{opt}(\omega - \Omega, z)\ \hat{E}_{THz}(\Omega, z)\ e^{-j\Delta k(\omega)z}d\Omega$$

$$+\mathcal{F}\left[j\frac{\varepsilon_0\omega_0\ n_{p,opt}^2\ n_2 d_{eff}}{2}\left|E_{opt}(t, z)\right|^2\ E_{opt}(t, z)\right] \tag{11.14}$$

$$+\mathcal{F}\left[j\frac{\varepsilon_0\omega_0\ n_{p,opt}^2\ n_2 d_{eff}}{2}\left[\left|E_{opt}(t - t', z)\right|^2 \otimes h_r(t')\right]\ E_{opt}(t, z)\right],$$
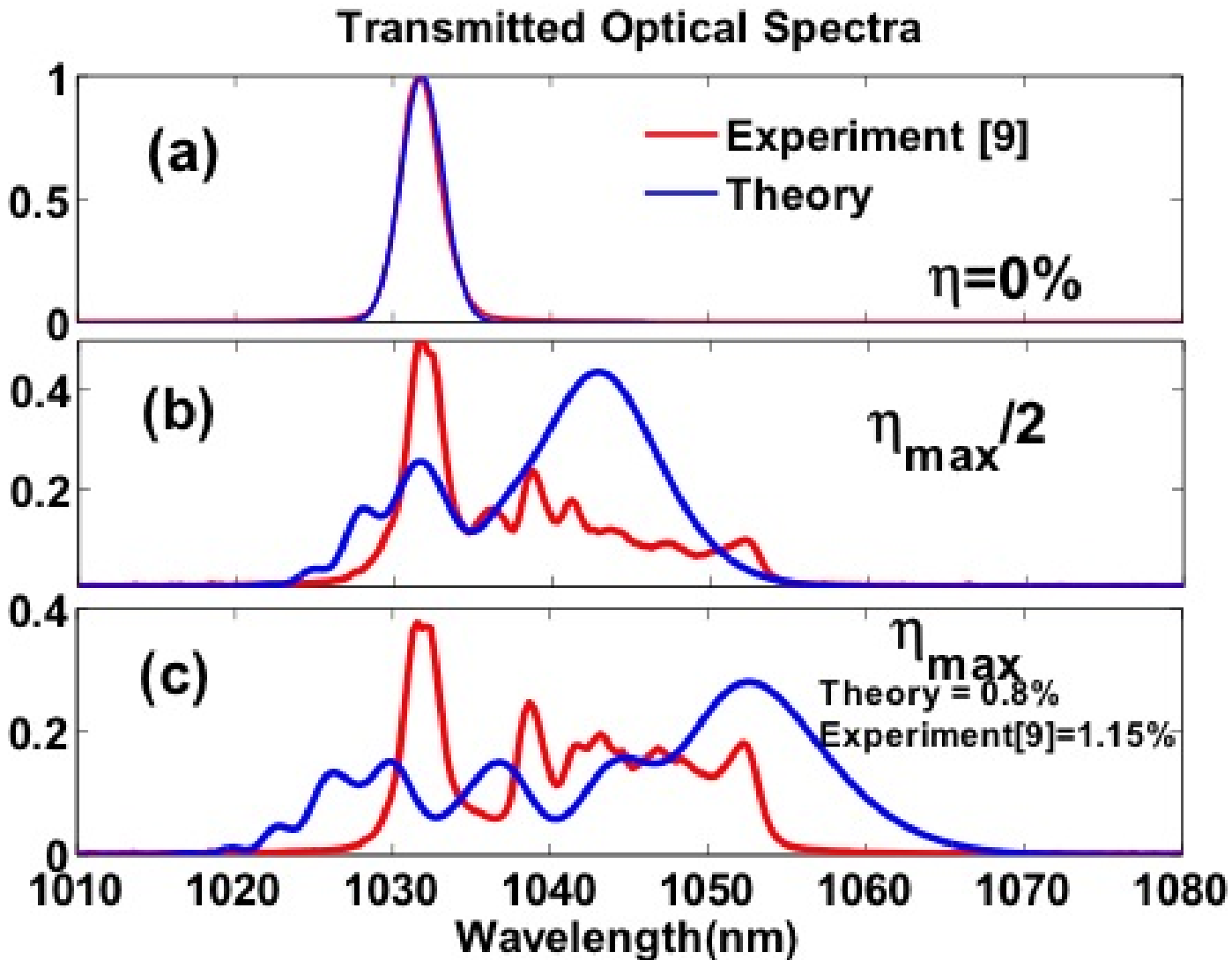
Figure 11.7: Comparison of experimental and simulated optical spectra for different amounts of generated THz.
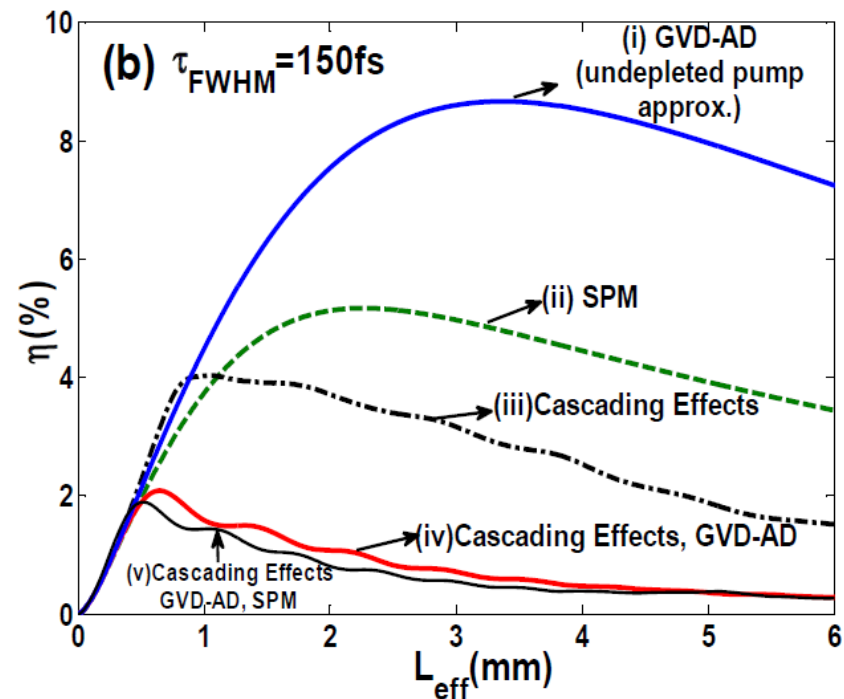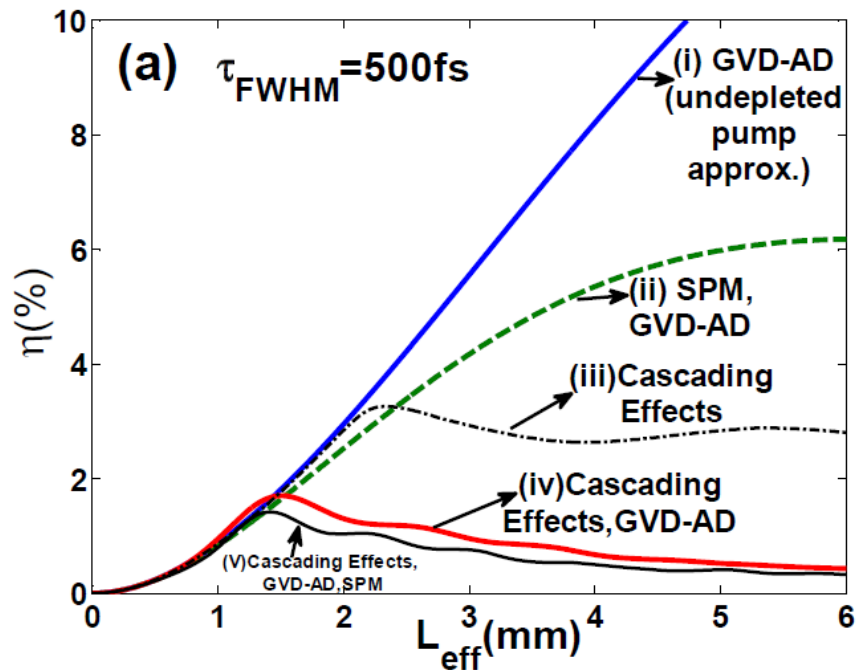
Figure 11.8: Conversion efficiencies as a function of effective length are calculated by switching on/off various effects. Material dispersion and absorption are considered for all cases. The pump fluence is 20 mJ/cm2, for a crystal temperature of 100 K. (a) Gaussian pulses with 500-fs FWHM pulse width with peak intensity of 40 GW/cm2 are used. Cascading effects together with GVD-AD leads to the lowest conversion efficiencies. The drop in conversion efficiency is attributed to the enhancement of phase mismatch caused by dispersion due to the large spectral broadening caused by THz generation (See Figs. 11.7(b)-(c)). However, since group velocity dispersion due to angular dispersion (GVD-AD) is more significant than GVD due to material dispersion at optical frequencies in lithium niobate, cascading effects in conjunc- tion with GVD-AD is the strongest limitation to THz generation. SPM effects are much less detrimental since they cause relatively small broadening of the optical pump spectrum (see 11.7 (a)). (b) Cascading effects along with GVD-AD are most detrimental even for a 150-fs Gaussian pulse with 3× larger peak intensity. [19]
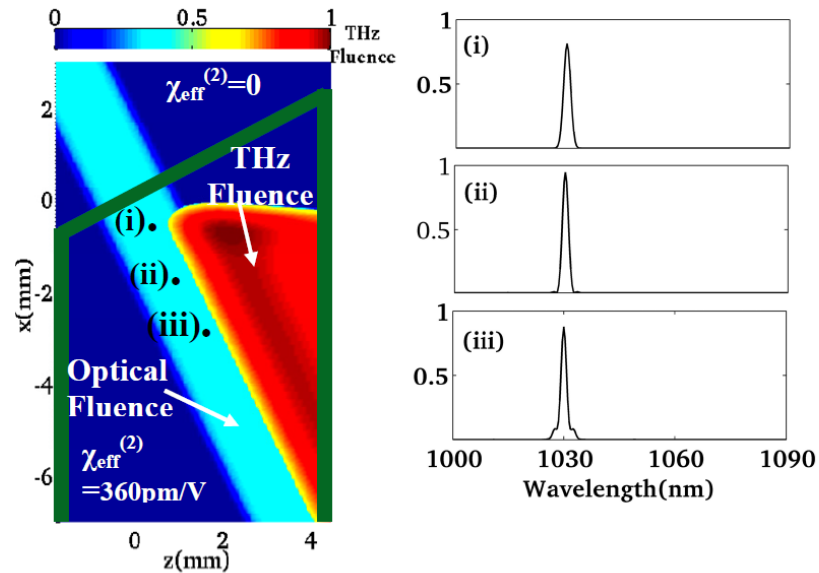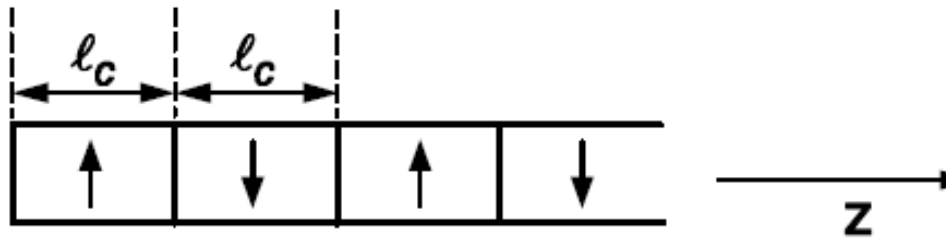
2D - Simulation
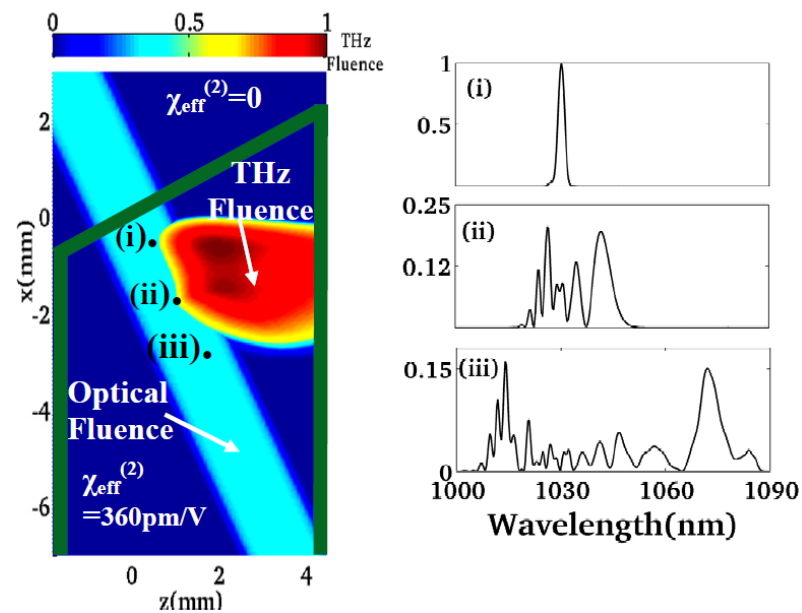
11.2.2 Optical rectification by Quasi-Phase Matching (QPM)

Periodically poled crystal

$$d_{eff}(z) = \sum_{m=-\infty}^{+\infty} d_m e^{jm\kappa z}$$

$$
\begin{aligned}
\Delta k &= \left. \frac{\partial k_{opt}(\omega)}{\partial \omega} \right|_{\omega_0} \Omega - k_{THz}(\Omega) + m\frac{2\pi}{\Lambda} = \left(\frac{1}{v_{g,opt}} - \frac{1}{v_{p,THz}} \right) \Omega + m\frac{2\pi}{\Lambda} \\
&= \left(\frac{n_{g,opt} - n_{p,THz}}{c} \right) \Omega + m\frac{2\pi}{\Lambda} = 0 \\
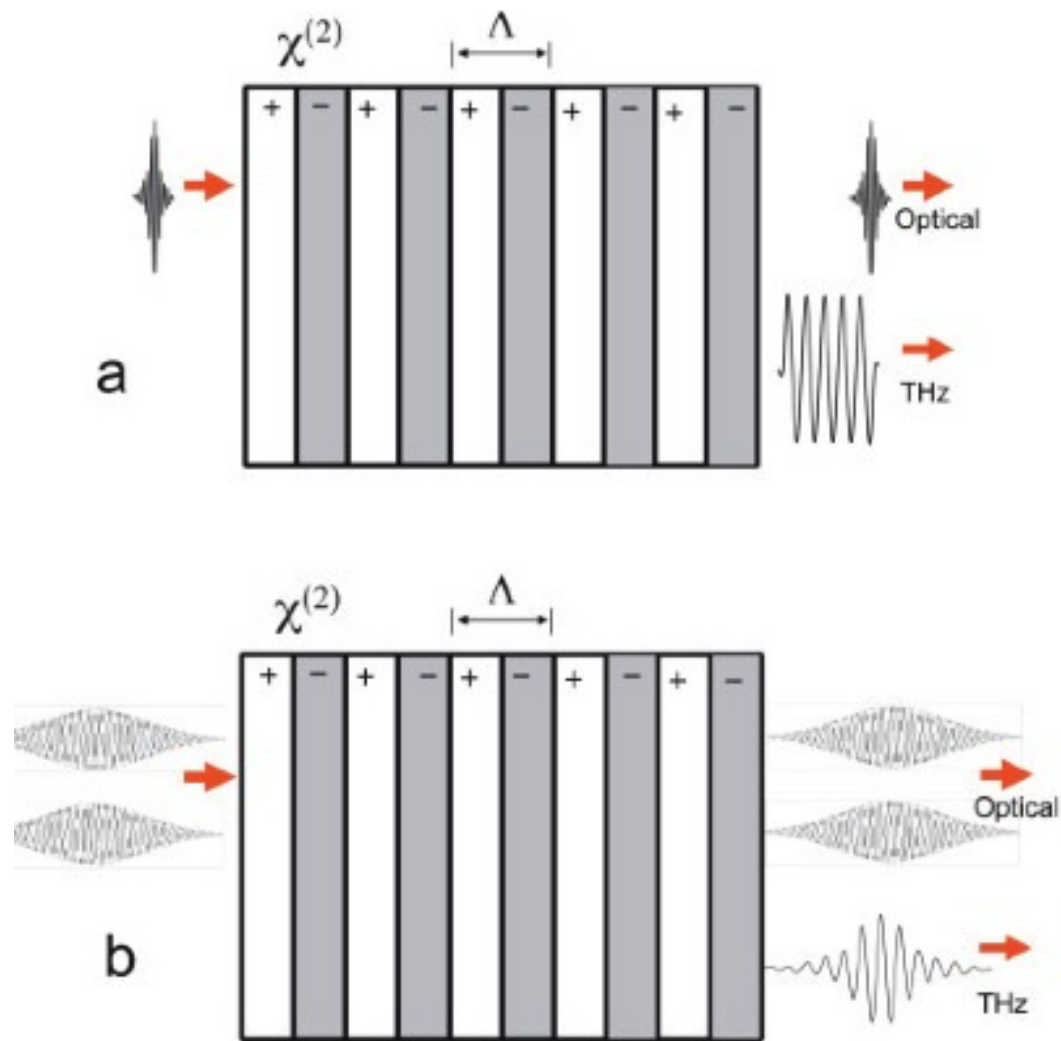\rightarrow \quad \Lambda &= m\frac{\lambda_{THz}}{n_{p,THz} - n_{g,opt}}.
\end{aligned}
$$

Figure 11.10: Schematic illustration of collinear THz-wave generation in a nonlin- ear crystal with periodically inverted sign of χ(2). (a) Optical rectification with femtosecond pulses, (b) difference-frequency generation with two picosecond pulses ($\Omega = \omega_3 - \omega_2$) [10].

Plane-wave analysis of optical-to-THz conversion in QPM crystals with ultrashort pulses

$$E_{opt}(t) = Re\{E_0 \, e^{-t^2/\tau^2} \, e^{j\omega_0 t}\} = \frac{1}{2}\{E_0 \, e^{-t^2/\tau^2} \, e^{j\omega_0 t} + c.c.\},$$

$$\hat{E}_{opt}(\omega) = \frac{E_o \tau}{2\sqrt{\pi}} \exp\left(-\frac{\tau^2 \omega^2}{4}\right)$$

$$
\begin{aligned}
\frac{d\hat{E}_{THz}(\Omega, z)}{dz} &= -j\frac{\Omega \, d_{eff}^{QPM}}{c \, n_{p,THz}} \frac{E_o^2 \tau^2}{4\pi} \int_{-\infty}^{+\infty} \exp\left(-\frac{\tau^2 (\omega + \Omega)^2}{4}\right) \exp\left(-\frac{\tau^2 \omega^2}{4}\right) d\omega \\
&= -j\frac{\Omega \, d_{eff}^{QPM}}{c \, n_{p,THz}} \frac{E_o^2 \tau}{2\sqrt{2\pi}} \exp\left(-\frac{\tau^2 \Omega^2}{8}\right) \, e^{j\Delta k(\Omega) z}. \quad (11.23)
\end{aligned}
$$

$$\left|\hat{E}_{THz}(\Omega, z)\right|^2 = \frac{\Omega^2 \, d_{eff}^{QPM,2}}{c^2 \, n_{p,THz}^2} \frac{E_o^4 \tau^2}{8\pi} \exp\left(-\frac{\tau^2 \Omega^2}{4}\right) \, L^2 \text{sinc}^2\left(\frac{\Delta k(\Omega) L}{2}\right) \quad (11.24)$$

$$\text{with } \Delta k(\Omega) = \Delta k = \frac{n_{g,opt} - n_{p,THz}}{c} + m\frac{2\pi}{\Lambda} \quad (11.25)$$

$$d_{eff}^{QPM} = \frac{2}{\pi} d_{eff}$$

Optical to THz conversion effficiency

$$\eta_{THz}^{PW} = \frac{\text{Fluence THz}}{\text{Fluence (pump)}}$$

$$F_{pump} = \frac{c\varepsilon_0 n_{p,opt}}{2} \int_{-\infty}^{+\infty} |E_{opt}(t,0)|^2 \, dt = \sqrt{\frac{\pi}{2}} \frac{c\varepsilon_0 n_{p,opt}}{2} E_o^2 \tau$$

and THz fluence

$$F_{THz} = \frac{c\varepsilon_0 n_{p,THz}}{2} \int_{-\infty}^{+\infty} |E_{THz}(t,L)|^2 \, dt = \frac{c\varepsilon_0 n_{p,THz}}{2} 2\pi \int_{-\infty}^{+\infty} \left| \hat{E}_{THz}(\Omega, z) \right|^2 d\Omega$$

(11.28)

where we used Parceval's theorem

$$\int_{-\infty}^{+\infty} |f(t)|^2 \, dt = 2\pi \int_{-\infty}^{+\infty} \left| \hat{f}(\Omega) \right|^2 d\Omega.$$

(11.29)

Thus, we obtain

$$\boxed{N = \frac{L}{\Lambda}}$$

$$\eta_{THz}^{PW} = \frac{\Omega^2 \, d_{eff}^{QPM,2} E_o^2 \tau}{2\sqrt{2\pi} c^2 \, n_{p,opt} n_{p,THz}} L^2 \int_0^{+\infty} \exp\left(-\frac{\tau^2 \Omega^2}{4} \right) \, \text{sinc}^2\left(\frac{\pi}{2} \frac{\Omega - \Omega_0}{\Delta\Omega}\right) d\Omega$$

(11.30)

with $\Omega_0 = \dfrac{2\pi \, c}{\Lambda\left(n_{g,opt} - n_{p,THz}\right)}$ and $\Delta\Omega = \dfrac{2\pi \, c}{L\left(n_{g,opt} - n_{p,THz}\right)} = \dfrac{\Lambda}{L}\Omega_0$ (11.31)

$$
\eta_{THz}^{PW,sp} = \frac{\Omega^2 \ d_{eff}^{QPM,2} E_o^2 c}{2\sqrt{2\pi}c^2 \ n_{p,opt}n_{p,THz}} \ L^2 g_1(\Omega_0) \ 2 \ \Delta\Omega =
$$

$$
= \frac{\Omega^2 \ d_{eff}^{QPM,2} E_o^2 \tau}{c \ n_{p,opt}n_{p,THz}} \ \frac{\sqrt{2\pi}}{(n_{g,opt} - n_{p,THz})} \ L \ g(\Omega_0)
$$

$$
= \frac{2\Omega^2 \ d_{eff}^{QPM,2} L}{\varepsilon_0 \ c^2 \ n_{p,opt}^2 n_{p,THz} \ (n_{g,opt} - n_{p,THz})} \ g_1(\Omega_0) \ F_{pump} \quad (11.32)
$$

$$
\text{with } g_1(\Omega_0) = \exp\left(-\frac{\tau^2\Omega_0^2}{4}\right) = \exp\left(-\left(\pi f_{THz}\tau\right)^2\right) \ \text{ and} \quad (11.33)
$$

$$
2 \ \Delta\Omega = \int_{-\infty}^{+\infty} \text{sinc}^2(\frac{\pi}{2}\frac{\Omega - \Omega_0}{\Delta\Omega}) \ d\Omega \quad (11.34)
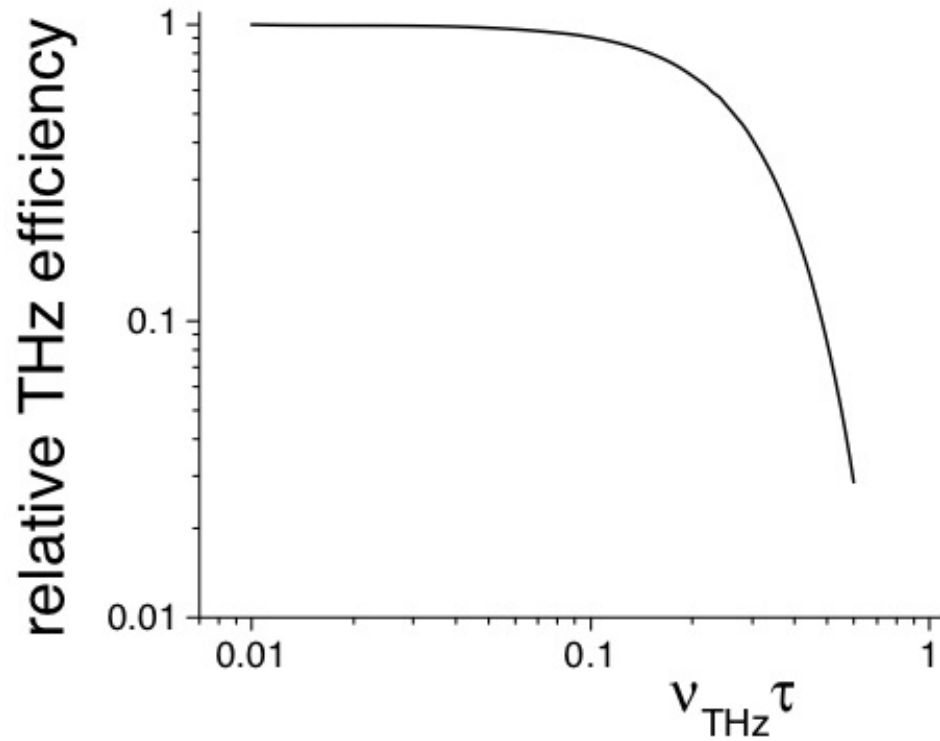$$

Influence of optical bandwidth

Figure 11.11: Relative THz generation reduction due to $g_1(\Omega_0)$.

For long pulses

$$\eta_{THz}^{PW,lp} = \frac{\Omega^2 \; d_{eff}^{QPM,2} E_o^2 \tau}{2\sqrt{2\pi}c^2 \; n_{p,opt}n_{p,THz}} L^2 \int_0^{+\infty} e^{\left(-\frac{\tau^2(\Omega-\Omega_0)^2}{4}\right)} \; \mathrm{sinc}^2(\frac{\pi}{2}\frac{\Omega-\Omega_0}{\Delta\Omega}) \; d\Omega. \quad (11.35)$$

$$= \frac{\Omega^2 \; d_{eff}^{QPM,2} E_o^2 \tau}{2\sqrt{2\pi}c^2 \; n_{p,opt}n_{p,THz}} L^2 \int_0^{+\infty} e^{\left(-\frac{\tau^2(\Omega')^2}{4}\right)} \; \mathrm{sinc}^2(\frac{\pi}{2}\frac{\Omega'}{\Delta\Omega}) \; d\Omega'. \quad (11.36)$$

Walk-off
$$l_w = \frac{\sqrt{\pi}c\tau}{(n_{g,opt} - n_{p,THz})}$$

$$\eta_{THz}^{PW,lp} = \frac{\Omega^2 \; d_{eff}^{QPM,2} E_o^2}{2\sqrt{2\pi}c^2 \; n_{p,opt}n_{p,THz}} L^2 \int_0^{+\infty} \exp^{\left(-\frac{y^2}{4}\right)} \; \mathrm{sinc}^2(\frac{\sqrt{\pi}}{2}\frac{L}{l_w}y) \; dy,$$

$$\eta_{THz}^{PW,lp} = \frac{\Omega^2 \; d_{eff}^{QPM,2} E_o^2}{\sqrt{2}c^2 \; n_{p,opt}n_{p,THz}} \frac{l_w L}{\pi} g_2(\frac{2l_w}{L})$$

$$g_2(x) = \int_0^{+\infty} \exp\left(-\frac{x^2\mu^2}{\pi}\right) \; \mathrm{sinc}^2(\mu) \; d\mu, \; \text{with } x = \frac{2l_w}{L}.$$
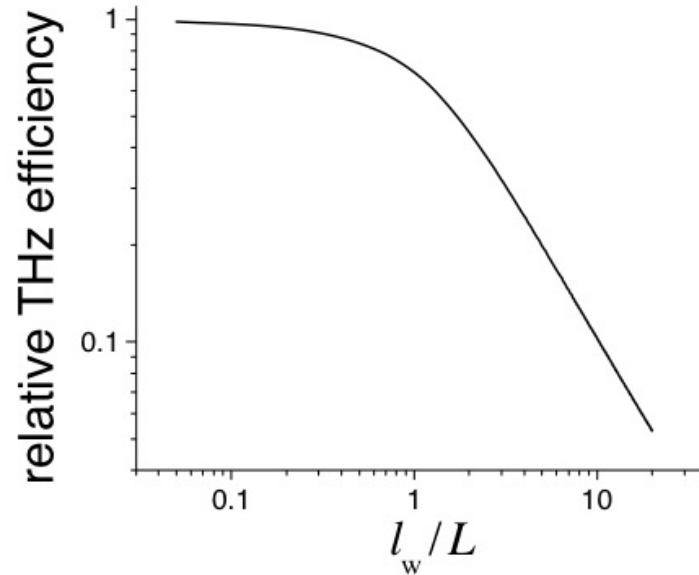
Influence of walk-off

Figure 11.12: Relative THz generation reduction due to $g_2(2\frac{l_w}{L})$.

Very long pulses

$$\eta_{THz}^{PW,lp\to\infty} = \frac{\Omega^2 \; d_{eff}^{QPM,2} E_o^2}{2\sqrt{2\pi}c^2 \; n_{p,opt}n_{p,THz}} L^2$$

$$= \frac{\Omega^2 \; d_{eff}^{QPM,2}}{\pi\varepsilon_0 c^3 \; n_{p,opt}^2 n_{p,THz}} \frac{F_{pump}}{\tau} L^2,$$

Optimal length of the EO crystal

$$\eta_{THz}(L) \sim \frac{1}{\alpha_{THz}} \left[1 - e^{-\alpha_{THz}L} \right] = L_{eff}$$

$$\eta_{THz}(L) \sim g_3 L, \text{ with } g_3 = \frac{1}{\alpha_{THz}L} \left[1 - e^{-\alpha_{THz}L} \right]$$

For $L = 1/\alpha_{THz}$, $g_3 = 0.63$.

Optimal focusing

$$\eta_{THz} = \frac{U_{THz}}{U_{pump}} = g_1 \ g_3 \ \frac{2\Omega^2 \ d_{eff}^{QPM,2} L}{\varepsilon_0 \ c^2 \ n_{p,opt}^2 n_{p,THz} \left(n_{g,opt} - n_{p,THz} \right)} \frac{U_{pump}}{\pi w^2}$$

$$\xi = (\lambda \ L / 2\pi n_{THz} w^2), \text{ where } \lambda \text{ is the THz wavelength}$$

Ratio between crystal length and THz Rayleigh range
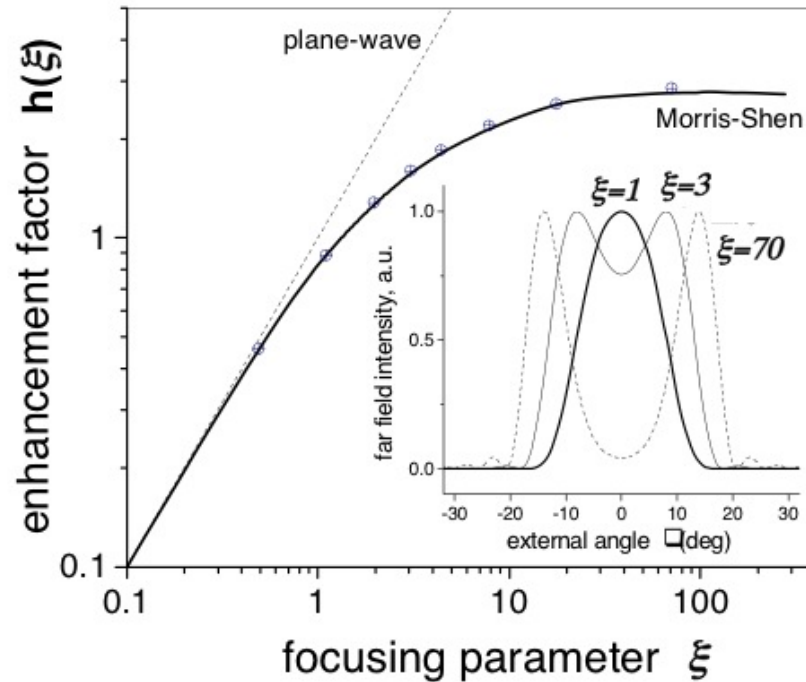
Enhancement factor

Figure 11.13: Enhancement factor h as a function of the focusing parameter ξ. Solid curve is based on Ref. [26]. Dashed curve – plane-wave approximation. Dots represent calculations based on the Green's function method. Inset: far-field THz intensity profiles at different ξ for a 1-cm-long GaAs.

Cascading and red shift

optical pulse spectrum will be red-shifted by $\Delta\omega/\omega_0 \sim \eta_{THz}$;
$N = 0.5 \times$ (acceptance bandwidth) / (terahertz frequency).

$$
\begin{aligned}
\frac{d\Delta k}{d\omega} &= \frac{\Omega}{c}\frac{dn_{g,opt}\left(\omega\right)}{d\omega} = \frac{\Omega}{c}\frac{dn_{g,opt}\left(\lambda\right)}{d\lambda}\frac{d\lambda}{d\omega} \\
&= \frac{\Omega}{c}\frac{dn_{g,opt}\left(\lambda\right)}{d\lambda}\frac{\lambda^2}{2\pi c}
\end{aligned}
$$

$$
\frac{d\Delta k}{d\omega}L\Delta\omega_{acc} = 2\pi
$$

$$
\Delta\omega_{acc} = \frac{2\pi c\omega}{L\Omega}\left(\lambda\frac{dn_{g,opt}\left(\lambda\right)}{d\lambda}\right)^{-1}.
$$

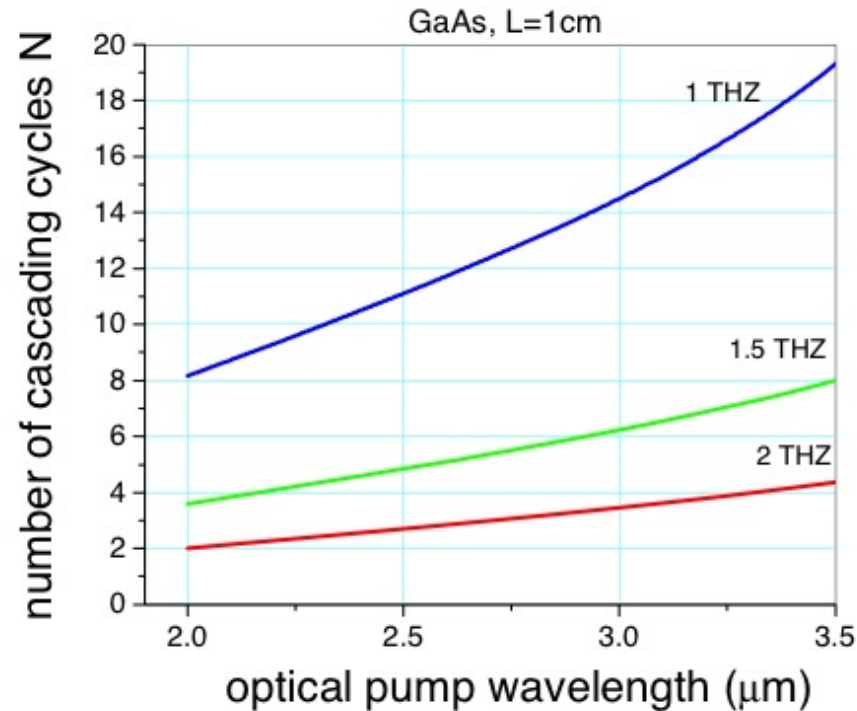# Cascading and red shift

Figure 11.14: Number of THz cascading cycles as a function of THz frequency and pump wavelength for GaAs, $L = 1$ cm.

Summary

$$FOM_1 = \frac{d_{eff}^2}{n_{p,opt}\alpha_{THz}} \tag{11.45}$$

or

$$FOM_2 = \frac{d_{eff}^2}{n_{p,opt}^2(n_{p,THz} - n_{g,opt})}. \tag{11.46}$$

If the maximum propagation distance is limited by the Kerr effect, the critical FOM becomes

$$FOM_3 = \frac{\lambda_{opt}\ d_{eff}^2}{n_{p,opt}^2 n_{p,THz}\alpha_{THz}n_2}. \tag{11.47}$$